IEEE Access
Multidisciplinary | Rapid Review | Open Access Journal

Received 26 July 2023, accepted 9 August 2023, date of publication 17 August 2023, date of current version 24 August 2023.

*Digital Object Identifier 10.1109/ACCESS.2023.3305944*

RESEARCH ARTICLE

# A New Technique for Improving the Precision of Dual-Axis Tetrahedron-Based Sensor With Switching Between PID and ANN

**YUWALDI AWAY[1], (Member, IEEE), ANDRI NOVANDRI[1], (Student Member, IEEE), ISYATUR RAZIAH[2], (Student Member, IEEE), AND MELINDA MELINDA[1], (Member, IEEE)**

[1]Department of Electrical and Computer Engineering, Universitas Syiah Kuala, Banda Aceh 23111, Indonesia
[2]Department of Information Technology, Universitas Teuku Umar, Meulaboh 23681, Indonesia

Corresponding author: Isyatur Raziah (isyaturraziah@utu.ac.id)

**ABSTRACT** This paper proposes a new technique for a dual-axis light tracking system using a combination of Proportional Integral Derivative (PID) and Artificial Neural Network (ANN) with a tetrahedron-based sensor. A tetrahedron-based sensor can detect the position of light using three photoresistor components arranged on a tetrahedron plane. The proposed technique combines PID and ANN controllers using a switching method that allows the algorithm to switch between PID and ANN based on the occurring errors. The updating of PID controller gains is done offline. Additionally, in the proposed tracking system, a new mechanism called dual-axis in dual-frame is introduced. This mechanism involves the use of two frames moving in parallel along opposite axes. Experimental results collected the angular movement data and the decrease in error values. Numerical analysis showed that the proposed prototype of the PID-ANN tracking system demonstrates better response time than previous prototypes mentioned in the literature. Moreover, this system also exhibits low error rates and improved data distribution. Therefore, the PID-ANN tracking system with the switching process enhances the performance of responsive, accurate, and precise light tracking.

**INDEX TERMS** Dual-axis, tetrahedron-based sensor, ANN, PID.

## I. INTRODUCTION

The tetrahedron-based sensor is a geometrically shaped sensor used for tracking light and determining its position. It can be applied in solar tracking systems with the aim of maximizing the potential electrical energy generated by solar panels [1], [2]. The tetrahedron-based sensor consists of three light sensor units in the form of photoresistors [3]. These sensors are attached to each face of the tetrahedron. The operation of this sensor involves comparing the differences in readings obtained from each photoresistor. Consequently, the sensor is capable of detecting and determining the coordinate position of the light source. The readings from the photoresistors can be obtained using a voltage divider circuit [4], [5] or a Wheatstone bridge circuit [6]. By implementing the appropriate sensor configuration, the tracking system can achieve accurate tracking and minimize errors. Furthermore, the use of a suitable sensor configuration can optimize the overall performance of the system [7].

The tetrahedron-based sensor technology remains popular to this day. This sensor technology was first introduced in the paper [8], which applied the sensor in a dual-axis solar tracking system. The study discussed in that paper focuses on the design and structure of the tetrahedron-based sensor, including the mechanisms involved in the dual-axis solar tracking system. The research aimed to identify the coordinate position of the sun based on sensor readings. The study of the tetrahedron-based sensor was also discussed in the paper [9]. This paper examined the influence of sensor dimension size on system performance. The research elaborated on how variations in sensor size can affect the overall performance of the tracking system. Furthermore, the paper [10] discusses the development of the tetrahedron-based sensor using a phototransistor. This research focuses on the use of

The associate editor coordinating the review of this manuscript and approving it for publication was Adamu Murtala Zungeru.

a phototransistor as a sensor component in the tracking system. The paper explains the implementation, characteristics, and advantages of using a phototransistor in the context of tetrahedron-based light tracking.

Furthermore, there are other literature discussing the advantages of tracking systems. One such literature identifies several advantages of tracking systems, as presented in the paper [11], which compares fixed-axis tracking systems with oriented-axis tracking systems. The study results indicate that oriented-axis tracking systems can produced 30% more electrical energy than fixed-axis systems. In paper [2], a study examines a solar tracking system designed in a mobile form, making the system a self-powering generator. The results show that oriented-axis tracking systems can increase energy by 67.65%. Meanwhile, in another study [12], the steward platform mechanism is utilized as an oriented-axis tracking system. Implementing the steward platform mechanism leads to a 32% increase in energy compared to fixed-axis systems. Based on these studies, oriented-axis tracking systems are preferred over fixed-axis systems. As discussed in the review article [13], the use of solar tracking systems is becoming increasingly popular as the utilization of solar energy as an alternative energy source continues to rise. The development of solar tracking systems continues, ranging from manual control using internet networks [14], [15] or bluetooth [16], and automatic control using a solar trajectory models [17], [18].

Artificial Neural Network (ANN) is an intelligent adaptive algorithm that can modify its variable structure to solve a problem based on the learned information [19], [20], [21]. The structure of an ANN consists of multiple nodes that form a network. Each node contains weight and bias variables. Since it belongs to supervised learning, the ANN algorithm requires training data to perform the learning process. The goal is to update the weight and bias variables based on the provided training data [22], [23], [24]. The accuracy of an ANN is determined based on the amount of training data and iterations that occur. The more iterations and training data, the more accurate the results [25], [26]. The application of ANN in tracker systems was discussed in the paper [27]. The study used a tetrahedron-based sensor to predict the sun's position in cloudy conditions. The training process was performed using 322 datasets and feed-forward backpropagation methods. The training process was carried out for 1000 iterations, resulting in the system's ability to predict the sun's position with a Mean Absolute Error (MAE) of 1.65 on the $x$-axis and 1.15 on the $y$-axis.

Proportional Integral Derivative (PID) is a closed-loop feedback control system that control stability in a system and minimize error values [28], [29]. The PID controller aims to improve the system's response time, including rise time, settling time, and overshoot. The PID controller has three main parameters: the proportional parameter, the integral parameter, and the derivative parameter. To obtain suitable PID parameters, a tuning process is necessary. The goal is to ensure that the system operates with the expected response time. Research on applying PID controllers in a prototype tracking system was discussed in paper [30], which utilized a tetrahedron-based sensor. The study's PID analysis resulted in an $x$-axis movement with an MAE value of 4.03 and a standard deviation of 3.31. Meanwhile, the $y$-axis movement obtained an MAE value of 1.2 and a standard deviation of 1.6.

Several studies have addressed the development of PID controllers used in tracking systems. In the paper [31], a simulation of a tracking system control using PID was conducted by modifying the Ziegler-Nichols Rules (PID-ZN). The modification resulted in faster system response time, with a rise time of 0.0176 seconds and a settling time of 0.0314 seconds, making the tracking system control more stable. In the subsequent paper [32], a simulation of tracking system control utilizing PID controllers with swarm intelligence optimization algorithms: Particle Swarm Optimization (PID-PSO), Cuckoo Search Algorithm (PID-CSA), and Firefly Algorithm (PID-FFA), was performed. The study revealed slow movement and deviation from the optimal point, leading to oscillation in the PID control. Furthermore, in the paper [33], which examined a prototype PID tracking system optimized with a Fuzzy Logic Controller (PID-FLC), the research results indicated a rise time of 3.6 seconds and a settling time of 4.8 seconds. The tracking system achieved an energy increase of 48.3% compared to the conventional tracking system.

Meanwhile, the development of PID-ANN algorithms has been discussed in several studies for specific applications, utilizing various different methods. Table 1 presents a literature review of the application of PID-ANN algorithms using different methods. Based on this literature review, it can be concluded that the PID-ANN algorithm has a significant impact on the system's response time. This algorithm is capable of providing better results in terms of aspects such as rise, delay, and settling times.

Through these studies, a new method based on the development of the PID-ANN algorithm for the tracking system is proposed to improve the response time. In this paper, a tetrahedron-based sensor is utilized as a light sensor to detect the direction and movement of light. To control the driving motor, the PID-ANN processing algorithm with a switching method is employed. The proposed method aims to switch between PID and ANN processing in order to optimize system performance. The PID controller plays a role in speeding up the response time, reducing oscillation as the motor approaches the target coordinates, and maintaining system stability. On the other hand, the adaptive ANN algorithm determines the motor rotation direction. Both algorithms are used alternately in the tracking system. When the sensor detects changes in the light position, the ANN algorithm is employed to adjust the tracking. Furthermore, when the system approaches the target point, the algorithm switches to PID control to ensure stable system performance and expedite target achievement.

The process of updating PID controller gains is done offline by adjusting control parameters before the system is executed. The proposed method demonstrates superior

**TABLE 1. Literature review of PID-ANN algorithm for different applications.**

| Paper | Year | Algorithm | Method | Application |
|---|---|---|---|---|
| Sandeep Gupta et al. [34] | 2023 | PID-ANN | ANN Self-Tuning PID | Step-up Power Converter |
| Najva Hassan et al. [35] | 2022 | PID-ANN | Adaptive Tuning | Wheeled Mobile Robots |
| Karrar H. Al-Waeli et al. [36] | 2021 | PID-ANN | ANN Self-Tuning PID | Lower Limb Exoskeleton |
| Omar Rodríguez-Abreo et al. [37] | 2021 | PID-ANN | ANN Self-Tuning PID | DC Motor Speed Control |
| K. Kumari et al. [38] | 2016 | PID-ANN | ANN Self-Tuning PID | Frequency of Power System |
| Rodrigo Hernández-Alvarado et al. [39] | 2016 | PID-ANN | ANN Self-Tuning PID | Underwater Vehicles Control |
| Chinenye Uchegbu et al. [40] | 2016 | PID-ANN | ANN Self-Tuning PID | Simulation Control Process |
| Shi-Gang Cui et al. [41] | 2013 | PID-ANN | ANN Self-Tuning PID | Mobile Robot Target Tracking |
| Muhammad Aamir [42] | 2013 | PID-ANN | ANN Self-Tuning PID | Robot Arm Control |
| Wei Lu et al. [43] | 2012 | ANN-DEA-PID | Hybrid Method | Simulation Control Process |
| M. Madheswaran el al. [44] | 2012 | PID-ANN | PID Self-Training ANN | Chopper Fed Embedded PMDC Motor |
| B. Vasu Murthy et al. [45] | 2012 | PID-ANN | ANN Self-Tuning PID | Liquid Level Control |
| O. A. Dahunsi et al. [46] | 2010 | PID-ANN | Adaptive Tuning | Hydraulic Vehicle Suspension Control |

results in terms of response time parameters, including rise time, settling time, and steady-state error. Additionally, to validate the research findings, a comparison is conducted between the proposed system and existing literature. The main contributions of this paper are as follows:

- We propose a tracking system with a new concept that utilizes the dual-axis in dual-frame mechanism. This concept involves the use of two frames moving in parallel along opposite axes to drive the tracking system in a dual-axis manner
- We propose the development of the PID-ANN algorithm by implementing a switching method. By utilizing this method, the tracking system can operate adaptively to achieve better response time results. Through the utilization of the PID-ANN algorithm and the ability to switch between them, the tracking system can adapt to different conditions and effectively optimize response time.
- The proposed tracking system is not limited to solar tracking, but is applicable to various types of tracking systems that utilize light as the monitored object.

## II. DESIGN SYSTEM

This paper proposes a dual-axis tracking system using a tetrahedron-based sensor. The explanation of the tetrahedron-based sensor design and the tracking system mechanism design are presented in this section.

### A. DESIGN OF TETRAHEDRON-BASED SENSOR

The tetrahedron-based sensor is a light-tracking sensor that works based on the principle of value comparison. The tetrahedron-based sensor is designed to resemble a three-sided pyramid shape and uses three photoresistors. The photoresistors are mounted on the sides of the tetrahedron as shown in Fig. 1. Meanwhile, Fig. 2. shows the geometric structure of the sensor, displaying the position points of each photoresistor defined as points $P_1$, $P_2$, and $P_3$.

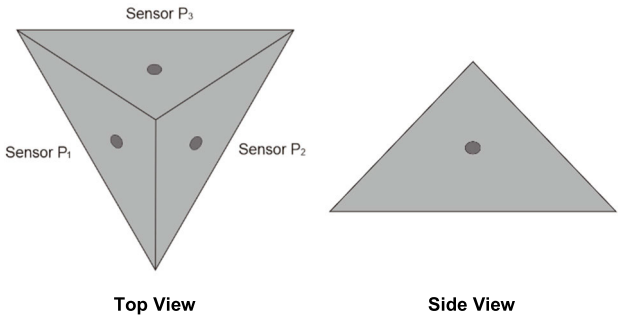


**FIGURE 1. Design of tetrahedron-based sensor.**

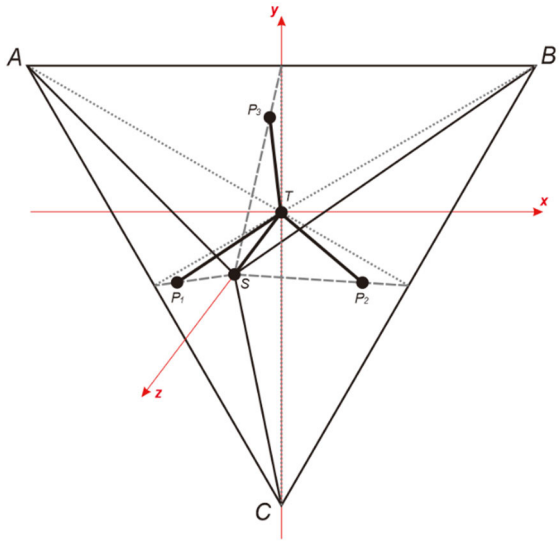


**FIGURE 2. Structure geometry of tetrahedron-based sensor.**

In Fig. 2, point $T$ is located at the center of the tetrahedron base, while point $S$ is located at the top of the tetrahedron. The coordinates of the center point can be calculated using

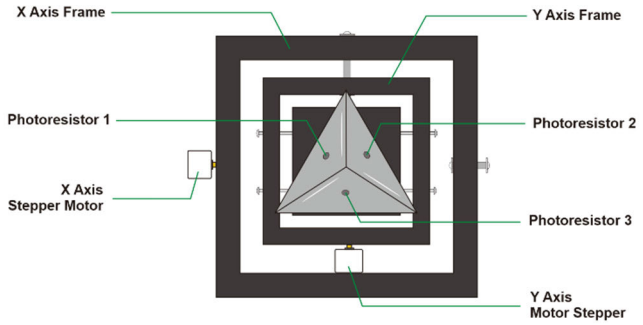


**FIGURE 3.** Design of tracker system.

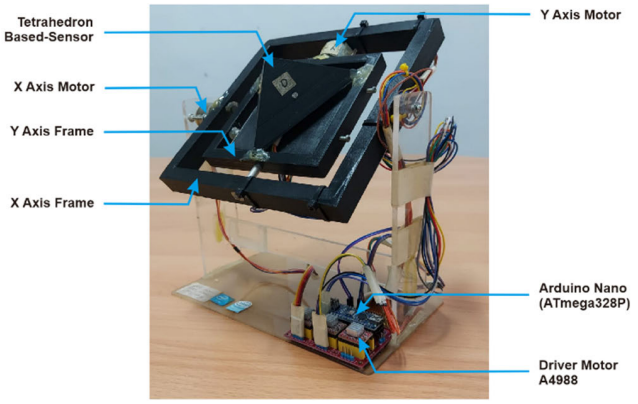


**FIGURE 4.** Proposed dual-axis tetrahedron-based sensor.

the centroid of triangle method. Based on the coordinates of points $A$, $B$, and $C$, the coordinates of point $T$ can be determined using the following equation,

$$\begin{bmatrix} x_T \\ y_T \\ z_T \end{bmatrix} = \begin{bmatrix} (x_A + x_B + x_C)/3 \\ (y_A + y_B + y_C)/3 \\ (z_A + z_B + z_C)/3 \end{bmatrix} \tag{1}$$

Meanwhile, to determine the coordinates of positions $P_1$, $P_2$, and $P_3$, the following equations are used,

$$\begin{bmatrix} x_{P1} \\ y_{P1} \\ z_{P1} \end{bmatrix} = \begin{bmatrix} (x_A + x_C + x_S)/3 \\ (y_A + y_C + y_S)/3 \\ (z_A + z_C + z_S)/3 \end{bmatrix} \tag{2}$$

$$\begin{bmatrix} x_{P2} \\ y_{P2} \\ z_{P2} \end{bmatrix} = \begin{bmatrix} (x_B + x_C + x_S)/3 \\ (y_B + y_C + y_S)/3 \\ (z_B + z_C + z_S)/3 \end{bmatrix} \tag{3}$$

$$\begin{bmatrix} x_{P3} \\ y_{P3} \\ z_{P3} \end{bmatrix} = \begin{bmatrix} (x_A + x_B + x_S)/3 \\ (y_A + y_B + y_S)/3 \\ (z_A + z_B + z_S)/3 \end{bmatrix} \tag{4}$$

### B. DESIGN OF TRACKER SYSTEM

The proposed design of the tracking system adopts the concept of dual-axis in dual-frame using two frames that move on different axes. This type of mechanism speeds up the system in tracking light because the motors work in parallel, meaning that both motors can be active simultaneously without waiting for the other motor to stop. The design of the tracking system is shown in Fig. 3. The outer frame is used to move the sensor on the $x$-axis, while the inner frame is used to move the sensor on the $y$-axis.

The result of the design is a physical device of a dual-axis tetrahedron-based sensor tracker system as shown in Fig. 4. The system uses an ATmega328P microcontroller and stepper motors as the drivers.

### C. MODEL MECHANISM OF TRACKER SYSTEM

The tracking system mechanism utilizes a tetrahedron-based sensor as the sensing device to detect the position of light. The operation principle of this system involves comparing the readings of each photoresistor, where $P_1$ serves as the reference. Based on these comparisons, the sensor can determine the light position on the $x$-axis and $y$-axis. The light position on the $x$-axis is determined by the difference in values between $P_1$ and $P_2$, while the light position on the $y$-axis is determined by the difference in values between $P_1$ and $P_3$. Thus, the difference in values can be expressed as follows,

$$e_x = |P_1 - P_3| \tag{5}$$

$$e_y = |P_1 - P_2| \tag{6}$$

where, $e_x$ represents the error value on the $x$-axis, and $e_y$ represents the error value on the $y$-axis.

The tetrahedron-based sensor is capable of detecting changes in the light position based on the brightness level read by the three photoresistors. When the brightness level at $P_1$ is lower than $P_2$, the $x$-axis motor moves in a clockwise (CW) direction. Conversely, if the brightness level at $P_1$ is higher than $P_2$, the $x$-axis motor moves in a counterclockwise (CCW) direction. Furthermore, when the brightness level at $P_1$ is lower than $P_3$, the $y$-axis motor moves in a CW direction. If the brightness level at $P_1$ is higher than $P_3$, the $y$-axis motor moves in a CCW direction. However, when all three photoresistors detect the same brightness level, both motors stop. This indicates that the tracking system has successfully oriented itself accurately towards the desired light source. During the tracking process, both motors are given equal priority because the system employs a parallel drive mechanism.

The mechanical system of the tracking system is depicted in Fig. 5. By applying Newton's First Law, the mathematical model can be expressed as follows,

$$\tau_1 - F_1.l \sin\theta_1 = 0 \tag{7}$$

$$\tau_2 - F_2.l \sin\theta_2 = 0 \tag{8}$$

where, $\tau_1$ represents the torque on the $x$-axis frame, $\tau_2$ represents the torque on the $y$-axis frame, $F_1$ represents the force on the $x$-axis frame, $F_2$ represents the force on the $y$-axis frame, $\theta_1$ represents the rotation angle on the $x$-axis, and $\theta_2$ represents the rotation angle on the $y$-axis. The flowchart illustrating the overall working principle of the tracking system is shown in Fig. 6.

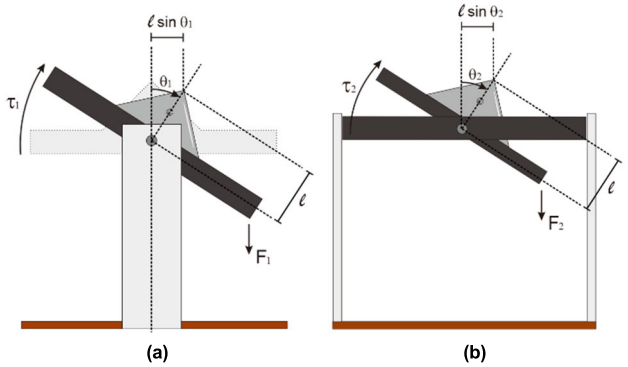


**FIGURE 5.** Mechanism of the tracking system; (a) x-axis movement; (b) y-axis movement.

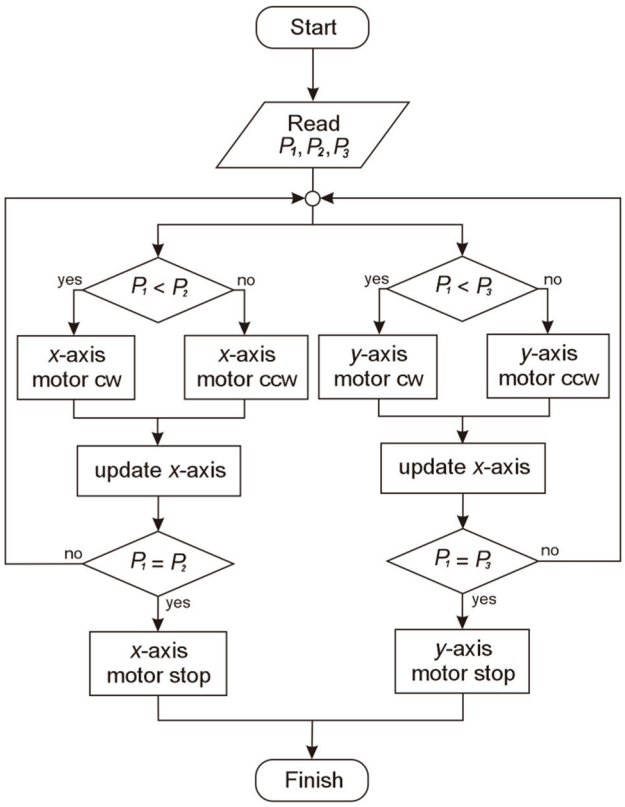


**FIGURE 6.** Flowchart of tracker system.

Meanwhile, to obtain the transfer function of the tracking system, it is derived by differentiating the mathematical model from Equation (7) and Equation (8). The derived results are expressed as follows,

$$I_1.\alpha_1 - m_1.g.l\sin\theta_1 = 0 \tag{9}$$
$$I_2.\alpha_2 - m_2.g.l\sin\theta_2 = 0 \tag{10}$$

where, $\alpha_1$ represents the angular acceleration on the $x$-axis frame, $\alpha_2$ represents the angular acceleration on the $y$-axis frame, $m_1$ represents the total mass of both tracker frames, $m_2$ represents the total mass of the $y$-axis frame, and $g$ represents the acceleration due to gravity. The parameters of the tracker device are presented in Table 2.

**TABLE 2.** Tracker parameters.

| Parameter | Value |
|---|---|
| $m_1\ (kg)$ | 0.147 |
| $m_2\ (kg)$ | 0.112 |
| $g\ (m/s^2)$ | 9.8 |
| $l\ (m)$ | 0.095 |

Next, Laplace transformation is performed, resulting in the following equation,

$$I_1.s^2\theta_1\ (s) - m_1.g.l\theta_1(s) = U_1(s) \tag{11}$$
$$I_2.s^2\theta_2\ (s) - m_2.g.l\theta_2(s) = U_2(s) \tag{12}$$

Therefore, the transfer function of the tracking system can be obtained as expressed below,

$$G_1\ (s) = \frac{\theta_1(s)}{U_1(s)} = \frac{1}{I_1.s^2 - m_1.g.l} \tag{13}$$
$$G_2\ (s) = \frac{\theta_2(s)}{U_2(s)} = \frac{1}{I_2.s^2 - m_2.g.l} \tag{14}$$

## III. PROPOSED PID-ANN ALGORITHM

The proposed system utilizes inputs in the form of $P_1$, $P_2$, and $P_3$ values. Meanwhile, the outputs are the movements of the motors along the $x$-axis and $y$-axis. In the proposed PID-ANN algorithm, there are several parameters that need to be considered. These parameters include the PID parameters and the ANN parameters.

### A. PID CONTROLLER MODEL

PID is a feedback control system that continuously calculates the error value as the difference between the desired setpoint and the measured process variable, utilizing gain values to adjust each parameter. The values of the three parameters have an impact on the system's response, stability, and can affect overshoot [47], [48]. In this study, the PID controller is tuned using the Ziegler-Nichols method. The tuning process of PID using the Ziegler-Nichols method involves gradually increasing the gain ($K_u$) and the time delay ($T_u$) until the system approaches the stability limit [49], [50]. Subsequently, the tuning process is carried out using the following equation,

$$K_p = 0.5K_u \tag{15}$$
$$T_i = 0.85T_u \tag{16}$$
$$T_d = 0.125T_u \tag{17}$$

where, the obtained value of $K_u$ is 9.6 and the value of $T_u$ is 1.42. Thus, the PID parameters are obtained as displayed in Table 3.

The general equation of the PID controller is defined as follows,

$$C\ (t) = K_p\left[e\ (t) + \frac{1}{T_i}\int e\ (t)\,dt + T_d\frac{de(t)}{dt}\right] \tag{18}$$

**TABLE 3.** PID parameters.

| Parameter | Value | Description |
|---|---|---|
| $K_p$ | 4.8 | Proportional gain |
| $T_i$ | 1.2 | Integral time constant |
| $T_d$ | 0.18 | Derivative time constant |

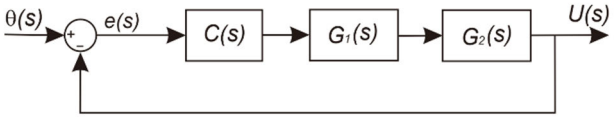


**FIGURE 7.** Block diagram of the PID system.

where, $K_p$, $T_i$, and $T_d$ are the main parameters of the PID controller that determine the response and stability of the system. Furthermore, the PID model is expressed as follows,

$$C(s) = K_p e(s)\left[1 + \frac{1}{T_i(s)} + T_d(s)\right] \tag{19}$$

where, $e(s)$ represents the difference between the setpoint variable $Y_{sp}(s)$ and the process variable $Y_m(s)$, which is defined as follows,

$$e(s) = Y_{sp}(s) - Y_m(s) \tag{20}$$

Fig. 7 illustrates the closed-loop control system of PID. $\theta(s)$ is the setpoint value of the desired angle. The output value of the PID is denoted $x_{pid}$ and $y_{pid}$.

### B. ANN MODEL

In ANN, there are two training stages to generate a model: Feed Forward and Back Propagation. In Feed Forward, the incoming data at the input layer is calculated at each node it passes through and then propagated until it reaches the output layer. Each calculation process at the nodes involves weight values, biases, and activation functions. The weight values are associated with the input node channels, while the biases are present at the nodes. The bias is a delta value used to correct the calculated results at the node. If no correction is needed, the bias is typically set to 0. The activation function acts as a non-linear filter, converting input signals into output signals. The type of activation function used depends on the problem being solved. In Back Propagation, the data at the output nodes is compared with the target data to determine the error. Based on the obtained error, the weight and bias are updated. These two stages are repeated until the appropriate error value is achieved.

Fig. 8 displays the ANN architecture with parameters explained in Table 4. In this architecture, there are $x$-axis motor represented as $m_x$ and $y$-axis motor represented as $m_y$.

In the ANN algorithm, there are several stages. First, calculating the value of the hidden node using the following equation,

$$H_x = \sum_{j=1}^{10}\sum_{i=1}^{3} I_i.w_{ij} + b_j; \quad 1 \le x \le 10 \tag{21}$$

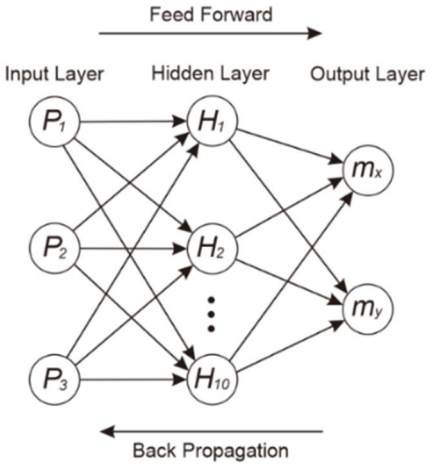


**FIGURE 8.** Proposed ANN architecture for tracker system.

**TABLE 4.** ANN parameters.

| Parameter | Value | Description |
|---|---|---|
| Number of layers | 3 | Number of layers in the ANN architecture |
| Number of input node | 3 | Number of nodes in the input layer |
| Number of hidden node | 10 | Number of nodes in the hidden layer |
| Number of output node | 2 | Number of nodes in the output layer |
| Number of iterations | 321 | Number of iterations in the training process |
| Learning rate | 0.3 | ANN learning rate parameter |
| Momentum factor | 0.9 | The parameters that affect weight changes |
| Error | 0.0005 | Maximum error value achieved after the learning process |
| Activation function of hidden layer | Sigmoid function | The type of activation function used in the hidden layer |
| Activation function of output layer | Sigmoid function | The type of activation function used in the output layer |
| Training method | Backpropagation | Training method used for the learning process |

where, $H_x$ represents the hidden value at node-$x$, $I_i$ represents the input value at node-$i$, $w_{ij}$ represents the weight value from input node-$i$ to hidden node-$j$, and $b_j$ represents the bias value at hidden node-$j$. Nodes in the hidden layer are defined as $j$, while nodes in the input layer are defined as $i$.

The activation function used is the sigmoid function, which is expressed in the following equation,

$$f(x) = \frac{1}{\left(1 + e^{-x}\right)}; \quad x = 1, 2, 3, \ldots, n \tag{22}$$

Next, the output value of the node is calculated using the following equation,

$$O_x = \sum_{k=1}^{2}\sum_{j=1}^{10} H_j.w_{jk} + b_k; \quad 1 \le x \le 2 \tag{23}$$

**TABLE 5.** Datasets.

| Data Input | | | Target | |
|---|---|---|---|---|
| $P_1$ | $P_2$ | $P_3$ | $m_x$ | $m_y$ |
| 5 | 5 | 5 | Stop | Stop |
| 5 | 5 | 0 | CCW | Stop |
| 5 | 0 | 5 | Stop | CW |
| 5 | 0 | 0 | CCW | CW |
| 0 | 5 | 5 | CW | CCW |
| 0 | 5 | 0 | Stop | CCW |
| 0 | 0 | 5 | CW | Stop |
| 0 | 0 | 0 | Stop | Stop |

where, $O_x$ represents the output value at node-$x$ and $H_j$ represents the hidden value at node-$i$. Nodes in the output layer are defined as $k$.

The values at the output node are then compared with the target data to determine the error value. The error can be calculated using Equation (24), where $T_{ij}$ represents the target data at node-$i$ and dataset-$j$, $O_i$ represents the output data of the network at node-$i$. The dataset used consists of eight data points displayed in Table 5. The input data consists of the minimum and maximum values of the photoresistors ($P_1$, $P_2$, $P_3$). The target data is grouped into three classes, representing commands to move both motors ($m_x$, $m_y$): CW, CCW, and Stop.

$$E = \sum_{j=1}^{8} \sum_{i=1}^{2} \frac{1}{2} \left(T_{ij} - O_i\right)^2 \tag{24}$$

The error value serves as a reference in the training process. When the error value reaches the predetermined threshold, the training process will stop. During this process, the weights and biases in each layer will be updated. To update the bias value at the output node, the following equation is used,

$$O_{bj} = \left(T_{ij} - O_j\right)\left(1 - O_j\right) O_j; \quad 1 \le j \le 2, \ 1 \le i \le 8 \tag{25}$$

where, $O_{bj}$ represents the output bias value at node-$j$, $T_{ij}$ is the target data at node-$j$ and dataset-$i$, $O_j$ is the output value at node-$j$.

Next, to update the weight value from the hidden layer to the output layer, the following equation is used,

$$O_{wij}(k+1) = \sum_{j=1}^{2} \sum_{i=1}^{10} \eta.H_i.O_{bj} + \delta.O_{wij}(k) \tag{26}$$

where, $O_{wij}$ represents the output weight value from the hidden layer at node-$i$ to the output layer at node-$j$, $\eta$ is the learning rate parameter, $H_i$ is the hidden value at node-$i$, $\delta$ is the momentum factor parameter, $k$ is the number of iterations that occur. The iteration value will continue to increase until the training process is completed.

Next, to update the bias value at the hidden node, the following equation is used,

$$H_{bj} = \left(1 - H_j\right).H_j.P; \quad 1 \le j \le 10 \tag{27}$$

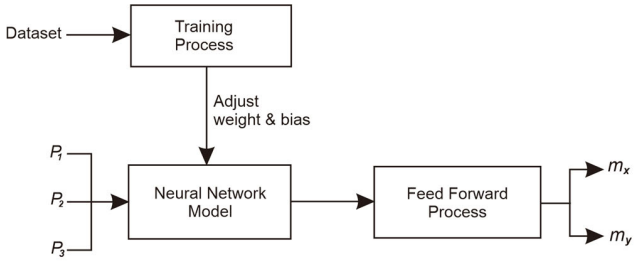


**FIGURE 9.** Block diagram of the ANN system.

where, $H_{bj}$ represents the hidden bias value at node-$j$, $H_j$ is the hidden value at node-$j$, and $P$ is the accumulation value of the output weight and output bias, which can be calculated using the following equation,

$$P = \sum_{j=1}^{10} \sum_{i=1}^{2} O_{wij}.O_{bi} \tag{28}$$

Next, to update the weight value from the input layer to the hidden layer, the following equation is used,

$$H_{wij}(k+1) = \sum_{j=1}^{10} \sum_{i=1}^{3} \eta.I_i.H_{bj} + \delta.H_{wij}(k) \tag{29}$$

where, $H_{wij}$ represents the hidden weight value from the input layer at node-$i$ ($1 \le i \le 3$) to the hidden layer at node-$j$ ($1 \le j \le 10$), and $I_i$ is the input value at node-$i$. Fig. 9 shows the overall block diagram of the ANN system. The output values from the ANN are denoted as $x_{ann}$ and $y_{ann}$.

The combination of PID-ANN algorithms is used to overcome the limitations of PID and can be used to replace conventional PID with the right configuration. PID acts as a controller to speed up the response time and smoothen the motor movement when approaching the target coordinates. The goal is to make the system responsive with reduced oscillations to maintain stability. In this system, an adaptive ANN algorithm is added, which functions as the determinant of motor rotation direction based on sensor readings. Through the backpropagation training process, the algorithm can understand patterns from the provided data and determine the motor's rotation direction. Both algorithms are used alternately with the switching method. The proposed method aims to switch between using PID and ANN for data processing. When the sensor detects a change in light position, the algorithm processes the data using ANN, making ANN act as the determinant of the rotation direction. Then, when the system is close to the target point, the algorithm switches to PID for processing. PID acts as a damper to reduce oscillations and maintain system stability. By combining PID and ANN, the tracking system can achieve minimum coordinate differences, short response times, and reduced oscillations when tracking the light source.

The proposed method of combining both PID-ANN algorithms utilizes a switching method between the PID controller and the ANN algorithms. Equation (30) is the method

used to control the movement of the tracking system in the $x$-axis, while Equation (31) is the method used to control the movement of the tracking system in the $y$-axis. The overall depiction of the proposed PID-ANN system is shown in the block diagram in Fig. 10. In this system, PID controller gains are updated offline, meaning control parameters are adjusted before the system is executed or during the preparation phase. This aims to optimize control performance and fine-tune settings before the system actually operates.

$$X = \begin{cases} x_{ann}, & if\ e_x > 0.8 \\ x_{pid}, & if\ 0 < e_x \leq 0.8 \\ 0, & otherwise \end{cases} \tag{30}$$

$$Y = \begin{cases} y_{ann}, & if\ e_y > 0.8 \\ y_{pid}, & if\ 0 < e_y \leq 0.8 \\ 0, & otherwise \end{cases} \tag{31}$$

## IV. PERFORMANCE ANALYSIS

The testing was conducted to observe the system's response in tracking light and to compare the performance of the proposed algorithm with the previous algorithms. The testing in this study used nine pieces of 5 watts LED lights with a light flux of 130 lumens. These lamps were positioned at different points.

Based on Fig. 11, the testing is conducted in three stages. In the first stage, the testing was conducted to observe the system's movement in tracking light at point $L_1$. In this stage, the system is tested to observe the response of the system in tracking the light in vertical movement, with the achieved angle $\theta_Y$, and the distance traveled $M_Y$. In the second stage, the testing was conducted to observe the system's movement in tracking light at point $L_2$. In this stage, the system is tested to observe the response of the system in horizontal movement, with the achieved angle $\theta_X$, and the distance traveled $M_X$. In the third stage, the testing was conducted to observe the system's movement in tracking light at point $L_3$. In this stage, the system is tested to observe the response of the system in diagonal movement, with the achieved angle $\theta_D$, and the distance traveled $M_D$. Through these tests, an analysis was conducted to obtain the performance results of the proposed tracking system. The coordinate positions of $L_1$, $L_2$, and $L_3$ are expressed in the following equation,

$$\begin{bmatrix} L_1 \\ L_2 \\ L_3 \end{bmatrix} = \begin{bmatrix} \cos\theta_Y.r_Y & \sin\theta_Y.r_Y & \cos\theta_Y \\ \cos\theta_X.r_X & \sin\theta_X.r_X & \cos\theta_X \\ \cos\theta_D.r_D & \sin\theta_D.r_D & \cos\theta_D \end{bmatrix} \tag{32}$$

Meanwhile, the angles achieved by the tracking system towards the light source are defined as $\theta_X$, $\theta_Y$, and $\theta_D$ expressed in the following equation,

$$\begin{bmatrix} \theta_X \\ \theta_Y \\ \theta_D \end{bmatrix} = \begin{bmatrix} arctan\left(M_X/z\right) \\ arctan\left(M_Y/z\right) \\ arctan\left(M_D/z\right) \end{bmatrix} \tag{33}$$

where, the values of $M_X$, $M_Y$, and $M_D$ can be calculated using the following equation,

$$\begin{bmatrix} M_X \\ M_Y \\ M_D \end{bmatrix} = \begin{bmatrix} \sin\theta_X.r_X \\ \sin\theta_Y.r_Y \\ \sin\theta_D.r_D \end{bmatrix} \tag{34}$$

The conducted analysis includes error analysis, motor response analysis, and accuracy and precision analysis. Error analysis is performed to determine the system's ability to minimize the occurring error. Meanwhile, motor response analysis is conducted to assess the stability and speed of the motor in responding to changes in light direction. The parameters measured in this stage include delay time, rise time, settling time, angular velocity, and lowest error deviation. Delay time represents the delay factor of the system's response measured until the response reaches 50% of the steady-state condition, rise time is the time it takes for the system's response to move from a stationary state to the setpoint, settling time is the time it takes for the system's response to reach 5% of the steady-state condition, and error deviation is a measure indicating the extent to which a system experiences deviations from the established standard value.

The subsequent analysis is the accuracy and precision analysis, which is performed to determine the accuracy and precision levels of each control algorithm used. The system's accuracy can be determined based on the error values. If the error value is low, the system is considered more accurate than the one system with a high error value. The commonly used methods for calculating error values are Mean Absolute Error (MAE) and Root Mean Squared Error (RMSE). These are calculated as follows,

$$MAE = \frac{1}{n}\sum_{i=1}^{n}\left|\theta_i - \hat{\theta}_i\right| \tag{35}$$

$$RSME = \sqrt{\frac{1}{n}\sum_{i=1}^{n}\left(\theta_i - \hat{\theta}_i\right)^2} \tag{36}$$

where, $n$ is the number of data points, $\theta_i$ represents the actual angle, and $\hat{\theta}_i$ represents the measured angle [51], [52].

Meanwhile, to determine the precision of the system, it can be assessed based on the parameter of the standard deviation. If the standard deviation value is low, the system is considered more precise than the system with a high standard deviation value [53], [54], [55]. The standar deviation is calculated using the following equation,

$$\sigma = \sqrt{\frac{\sum_{i=1}^{n}(x_i - \mu)^2}{n}} \tag{37}$$

where, $\sigma$ represents the standard deviation value and $\mu$ represents the mean value, which can be calculated using the following equation,

$$\mu = \frac{1}{n}\sum_{i=1}^{n} x_i \tag{38}$$

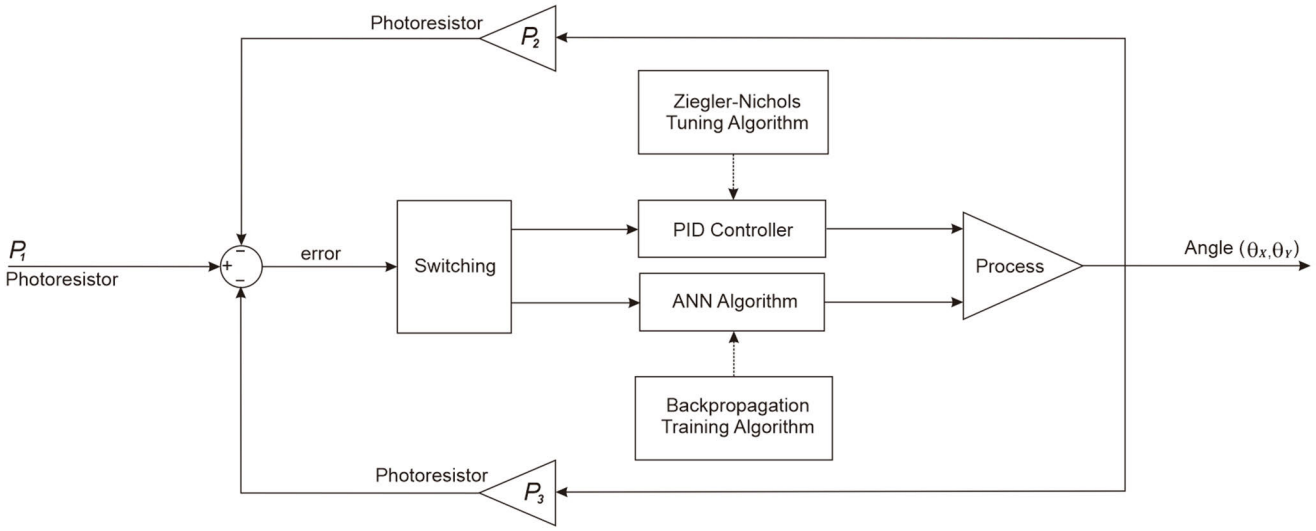


**FIGURE 10.** Block diagram of the proposed PID-ANN tracking system.

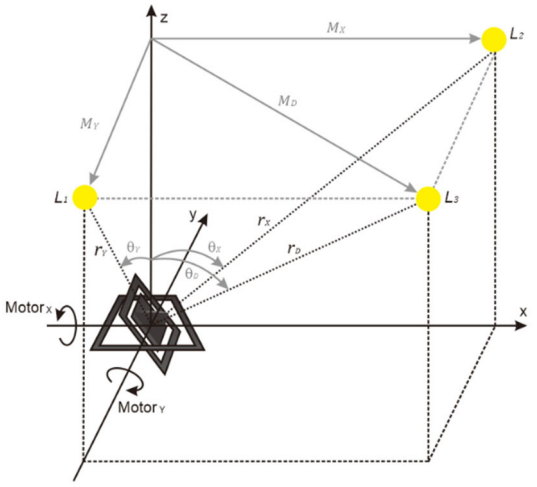


**FIGURE 11.** System testing method.

where, $x_i$ represents the value at data point-$i$ and $n$ represents the number of data points.

Then, to determine the data density in each system, an analysis is conducted using a normal distribution obtained by calculating the Probability Density Function (PDF). Before calculating the PDF, data normalization is performed to ensure that all data have the same scale. The normalization method used is the max-min method, which scales the data between 0 and 1. The data normalization process is carried out using the following equation,

$$\hat{x} = \frac{x - x_{min}}{x_{max} - x_{min}} \tag{39}$$

where, $\hat{x}$ is the normalized data and $x$ is the original data. The value $x_{min}$ represents the minimum value of a set of original data, while $x_{max}$ represents the maximum value of the same set of original data [56].

Next, based on the normalized data, the value of PDF can be calculated using the following equation [57],

$$f(x) = \frac{1}{\sigma\sqrt{2\pi}} e^{-\frac{1}{2}\left(\frac{x-\mu}{\sigma}\right)^2} \tag{40}$$

## V. RESULTS AND DISCUSSION

In this paper, the goal is to determine the performance level of the proposed PID-ANN algorithm on the dual-axis tetrahedron-based sensor system, which includes delay time, rise time, settling time, angular velocity, and lowest error deviation. Additionally, to compare the proposed PID-ANN algorithm with previous research that has been conducted.

### A. SYSTEM PERFORMANCE WITH PID-ANN ALGORITHM

This testing is conducted to evaluate the performance of the tracking system by implementing the proposed PID-ANN algorithm. The evaluation is done to observe the movement of the motors on the $x$-axis and $y$-axis in detecting changes in the light position. When there is a change in the light position, the error value will increase. In this condition, the system will attempt to minimize the error by moving both motors until it reaches the minimum value. The error values are then plotted into graphs. Through the visualization of these graphs, information regarding response time and motor speed can be obtained. The testing is performed under three conditions: when there are vertical, horizontal, and diagonal changes in the light position. Furthermore, an analysis is conducted to gain a deeper understanding of the responsiveness and performance of the tracking system in responding to changes in the light position from different directions.

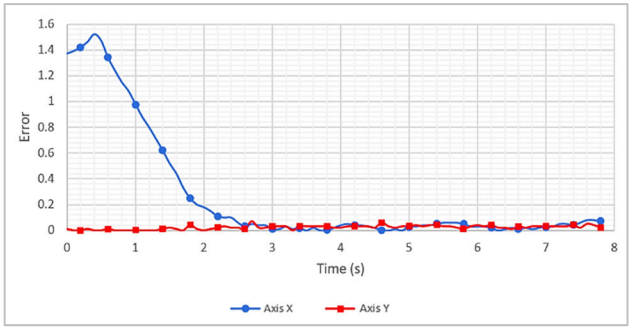


**FIGURE 12.** Experiment results on the vertical displacement of light.

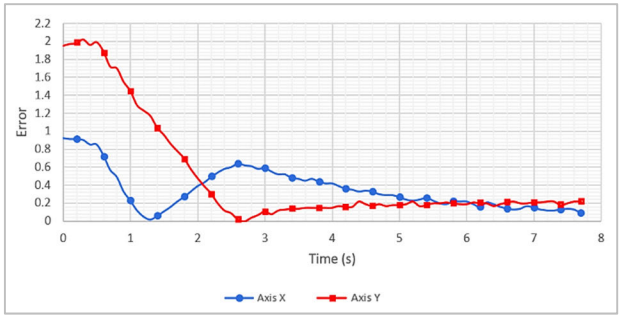


**FIGURE 13.** Experiment results on the horizontal displacement of light.

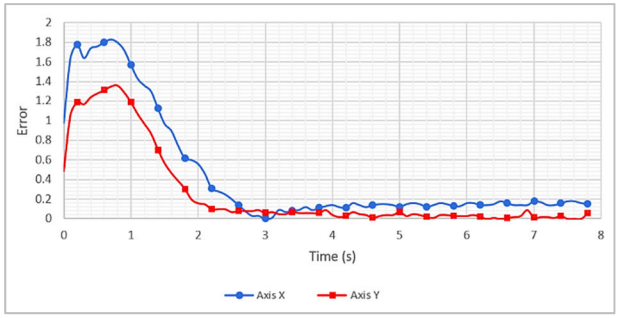


**FIGURE 14.** Experiment results on the diagonal displacement of light.

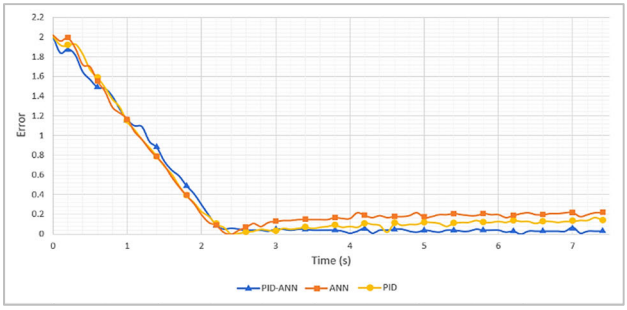


**FIGURE 15.** The comparison of error values between the proposed PID-ANN algorithm with PID and ANN algorithms.

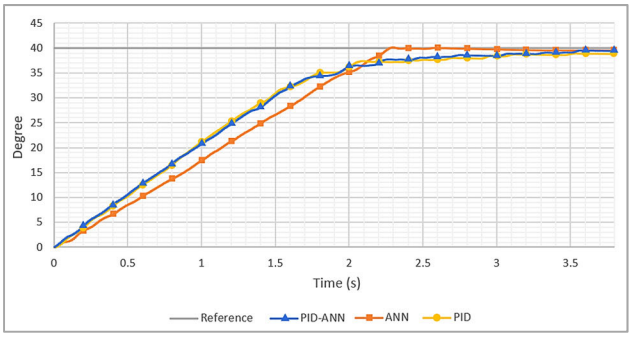


**FIGURE 16.** The comparison of response system between the proposed PID-ANN algorithm with PID and ANN algorithms.

The test results for the vertical light displacement are displayed in Fig. 12. Based on the graph, it can be observed that when the sensor detects the light, there is an error on the $x$-axis. This is because sensor $P_3$ detects brighter light than sensors $P_1$ and $P_2$. Consequently, the $x$-axis motor moves to reduce the error. The time taken for the $x$-axis motor to reach the highest error is 2.6 seconds. The $x$-axis motor can stabilize at a lowest error of 0.07, while the $y$-axis motor stabilizes at 0.02.

Next, the graph of the test results for horizontal light displacement is displayed in Fig. 13. Based on the graph, it can be observed that both motors move in opposite directions. The $x$-axis motor moves for 1.3 seconds to reach the setpoint and then moves back. Meanwhile, the $y$-axis motor moves for 2.7 seconds. The $x$-axis motor can stabilize at a highest error of 0.09, while the $y$-axis motor stabilizes at 0.22.

Next, the graph of the test results for diagonal light displacement is displayed in Fig. 14. Based on the graph, it shows that both motors move in opposite directions. The $x$-axis motor moves for 3 seconds to reach the setpoint. Meanwhile, the $y$-axis motor moves for 4 seconds. The $x$-axis motor can stabilize at a highest error of 0.15, while the $y$-axis motor stabilizes at 0.06.

### B. SYSTEM PERFORMANCE COMPARISON

The system comparison is conducted to determine the performance comparison of the proposed PID-ANN algorithm. In the initial testing, the comparison is carried out using the same tracking device between the proposed PID-ANN tracking system and two other algorithms: the PID algorithm and the ANN algorithm. Fig. 15 shows the graph of the error values when the system detects light displacement. Meanwhile, Fig. 16 shows the graph of the system's movement in tracking light displacement.

Table 6 presents the comparison data obtained from the results of both graphs. The proposed PID-ANN tracking system achieves smaller delay time and rise time, allowing the system to reach the setpoint quickly. However, the system could not reach steady-state conditions quickly, as seen from the settling time obtained, which is 2.46 seconds, 0.23 seconds slower than the ANN. The proposed PID-ANN tracking system achieves an angular velocity of 21.12 deg/s with a lowest error deviation of only 0.07.

**TABLE 6.** The result comparison of response system.

| Algorithm | Delay Time (s) | Rise Time (s) | Settling Time (s) | Angular Velocity (deg/s) | Steady State Error |
|---|---|---|---|---|---|
| PID-ANN (Proposed) | 1.09 | 2.18 | 2.46 | 21.12 | 0.07 |
| ANN | 1.11 | 2.22 | 2.23 | 17.35 | 0.22 |
| PID | 1.1 | 2.20 | 2.92 | 20.18 | 0.17 |

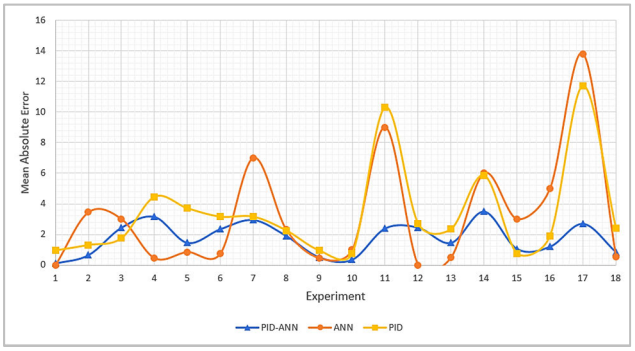


**FIGURE 17.** The comparison of mean absolute error between the proposed PID-ANN algorithm with PID and ANN algorithms.

Based on the test results, it can be concluded that the proposed tracking system mechanism remains stable under the control of PID-ANN, PID, and ANN. The test results demonstrate that the proposed tracking system mechanism can maintain stability in responding to changes in light position and effectively preserve system stability, regardless of the type of controller used.

The next analysis is about accuracy using the MAE and RMSE parameters, including precision analysis using the standard deviation parameter. The testing process was conducted 18 times with a randomized light source position. Fig. 17 shows the graph of the MAE comparison results. Based on the graph, the proposed PID-ANN tracking system has relatively low MAE values than other tracking systems, with a maximum value of 3.5. Meanwhile, the normal distribution comparison is plotted in Fig. 18. The curve shows that the proposed PID-ANN tracking system has a narrower curve than other tracking systems, indicating that the data spread in the PID-ANN testing is smaller.

Based on the testing process, the system performance data is compared in Table 7. The data shows that the proposed PID-ANN tracking system has the lowest parameter values. Based on the obtained comparison results, it can be concluded that the proposed PID-ANN tracking system has better accuracy and precision compared to individual PID and ANN tracking systems. This indicates that the combination of PID and ANN in the tracking system can result in better performance in tracking light movements.

Furthermore, to validate the proposed PID-ANN algorithm, a comparison was made with algorithms from other relevant literature concerning the prototype results of the tracking system. The compared algorithms include

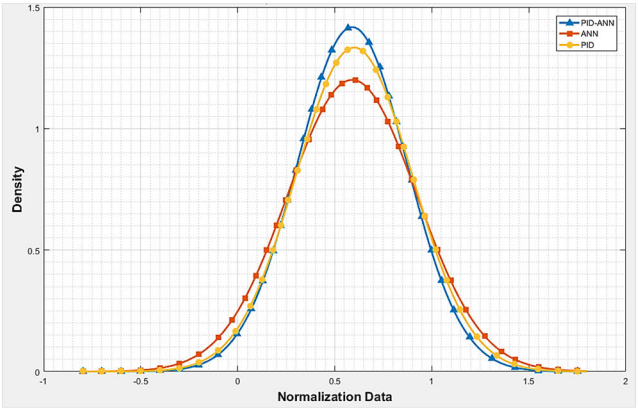


**FIGURE 18.** The comparison of normal distribution between the proposed PID-ANN algorithm with PID and ANN algorithms.

**TABLE 7.** The result comparison of performance system.

| Algorithm | MAE | RMSE | Standard Deviation |
|---|---|---|---|
| PID-ANN (Proposed) | 1.75 | 2.61 | 0.2815 |
| ANN | 3.17 | 4.85 | 0.3324 |
| PID | 3.35 | 4.81 | 0.2992 |

**TABLE 8.** The comparison of the proposed PID-ANN algorithm with other published algorithms.

| Algorithm | Rise Time (s) | Settling Time (s) | Steady State Error |
|---|---|---|---|
| PID-ANN (Proposed) | 2.18 | 2.46 | 0.07 |
| PID | 2.2 | 6.6 | 1.2 |
| IMC | 3.38 | 9 | 2 |
| ABC | 2.37 | 5.23 | 1.05 |
| PID-IMC | 1.8 | 5.58 | - |
| PID-CHR | 4 | 5.59 | - |
| PID-ZN | 6.55 | 6.9 | - |
| PID-TL | 9.38 | 10.1 | - |
| PID-FLC | 3.6 | 4.8 | 0.4 |
| PD-FLC | 6.38 | 6.38 | 0.83 |

PID controller [30], Internal Model Controller (IMC) [58], Artificial Bee Colony (ABC) [59], PID with Internal Model Controller (PID-IMC), PID with Chien-Hrones-Reswick (PID-CHR), PID with Ziegler-Nichols (PID-ZN), PID with Tyreus-Luyben (PID-TL) [60], PID with Fuzzy Logic Controller (PID-FLC) [33], and PD with Fuzzy Logic Controller (PD-FLC) [61]. The performance of the tracking system was analyzed through a comparison as shown in Table 8. The comparison parameters include response time, which consists of rise time, settling time, and steady-state error. Based on the conducted comparison, the proposed PID-ANN algorithm demonstrates a better response time than the existing algorithms. This indicates that the PID-ANN algorithm has an advantage in accelerating the response time of the tracking system. With a smaller response

time, the tracking system can provide quicker responses to the movements of the light source. This can enhance the overall performance and efficiency of the tracking system.

## VI. CONCLUSION

The proposed system is a tracker with the latest design and mechanism by applying tetrahedron-based sensor technology into the dual-axis in dual-frame concept with a combination of PID-ANN algorithm developed by adding a switching method. The results showed that the proposed PID-ANN tracker system has the highest angular velocity, 21.12 deg/s, with the lowest error deviation, 0.07. In the accuracy analysis comparison, the proposed PID-ANN tracker system obtained lower MAE and RMSE values, 1.75 and 2.61 respectively, than other tracking systems. Meanwhile, in the precision analysis comparison, the proposed PID-ANN tracker system obtained a lower standard deviation value of 0.2815 than other tracking systems. Therefore, the proposed PID-ANN tracker system has higher accuracy and precision than the ANN and PID tracker systems. Thus, this proposed PID-ANN tracker system can accurately and responsively track light movement to obtain a minimum error.

Although the proposed PID-ANN algorithm has several advantages, there are some limitations that need to be considered, such as limited response speed. While the PID-ANN algorithm can accelerate the response time than conventional PID, its response speed is still limited by the ANN algorithm. ANN algorithms require more time for learning and adaptation processes before providing accurate responses. Additionally, this tracking system is highly dependent on the quality and reliability of the sensors used. Inaccurate or vulnerable sensors can affect the accuracy and stability of the tracking system.

In future work, there will be further development and enhancement of the PID-ANN algorithm, taking into account aspects such as parameter tuning, more adaptive switching methods, improved adaptability, and integration with new sensor technologies.

## ACKNOWLEDGMENT

The authors would like to thank the LPPM of Universitas Syiah Kuala for funding this research.

## REFERENCES

[1] D. M. Ajay, B. P. Ajit, H. P. Prajot, and S. S. Kiran, "Design and fabrication of dual axis solar tracker for maximum energy harvesting," *Int. J. Res. Publ. Eng. Technol.*, vol. 1, no. 1, pp. 1–4, 2015.

[2] Y. R. Al-Saadi, M. S. Tapou, A. A. Badi, S. Abdulla, and M. Diykh, "Developing smart self orienting solar tracker for mobile PV power generation systems," *IEEE Access*, vol. 10, pp. 79090–79099, 2022, doi: 10.1109/ACCESS.2022.3194026.

[3] G. Prinsloo and R. Dobson, *Solar Tracking: High Precision Solar Position Algorithms, Programs, Software and Source-Code for Computing the Solar Vector, Solar Coordinates & Sun Angles in Microprocessor, PLC, Arduino, PIC and PC-Based Sun Tracking Devices or Dynamic Sun Following Hardware*. Stellenbosch, South Africa: SolarBooks, 2015.

[4] A. E. Hammoumi, S. Motahhir, A. E. Ghzizal, A. Chalh, and A. Derouich, "A simple and low-cost active dual-axis solar tracker," *Energy Sci. Eng.*, vol. 6, no. 5, pp. 607–620, Oct. 2018, doi: 10.1002/ese3.236.

[5] S. Motahhir, A. El Hammoumi, A. El Ghzizal, and A. Derouich, "Open hardware/software test bench for solar tracker with virtual instrumentation," *Sustain. Energy Technol. Assessments*, vol. 31, pp. 9–16, Feb. 2019, doi: 10.1016/j.seta.2018.11.003.

[6] M. Saeedi and R. Effatnejad, "A new design of dual-axis solar tracking system with LDR sensors by using the wheatstone bridge circuit," *IEEE Sensors J.*, vol. 21, no. 13, pp. 14915–14922, Jul. 2021, doi: 10.1109/JSEN.2021.3072876.

[7] S. I. Palomino-Resendiz, F. A. Ortiz-Martínez, I. V. Paramo-Ortega, J. M. González-Lira, and D. A. Flores-Hernández, "Optimal selection of the control strategy for dual-axis solar tracking systems," *IEEE Access*, vol. 11, pp. 56561–56573, 2023, doi: 10.1109/ACCESS.2023.3283336.

[8] Y. Away and M. Ikhsan, "Dual-axis sun tracker sensor based on tetrahedron geometry," *Autom. Construct.*, vol. 73, pp. 175–183, Jan. 2017, doi: 10.1016/j.autcon.2016.10.009.

[9] H. A. Lastya, Y. Away, T. Tarmizi, I. D. Sara, and M. Ikhsan, "Effect difference size of tetrahedron sun tracker based on sensor for energy harvesting," in *Proc. Int. Conf. Comput. Sci., Inf. Technol. Eng. (ICCoSITE)*, 2023, pp. 111–116, doi: 10.1109/ICCoSITE57641.2023.10127761.

[10] H. A. Lastya, Y. Away, I. D. Sara, M. Ikhsan, and N. M. Mirdha, "Development of dual-axis sun tracker based on tetrahedron geometry using phototransistor sensor," in *Proc. Comput. Electr. Educ. Res. (PROCESSOR)*, 2023, pp. 91–102.

[11] J. Doss, M. Kumaravel, and V. J. Kumar, "A novel measurement technique for performance comparison of sun tracker systems," in *Proc. IEEE Int. Instrum. Meas. Technol. Conf. (IMTC)*, May 2013, pp. 1156–1160, doi: 10.1109/I2MTC.2013.6555595.

[12] M. Engin, "Controller design for parallel mechanism solar tracker," *Machines*, vol. 11, no. 372, pp. 1–17, 2023, doi: 10.3390/machines11030372.

[13] A. Musa, E. Alozie, S. A. Suleiman, J. A. Ojo, and A. L. Imoize, "A review of time-based solar photovoltaic tracking systems," *Information*, vol. 14, p. 211, Mar. 2023, doi: 10.3390/info14040211.

[14] K. Kumar, L. Varshney, A. Ambikapathy, V. Mittal, S. Prakash, P. Chandra, and N. Khan, "Soft computing and IoT based solar tracker," *Int. J. Power Electron. Drive Syst.*, vol. 12, no. 3, pp. 1880–1889, 2021, doi: 10.11591/ijpeds.v12.i3.pp1880-1889.

[15] S. Aziz and M. Hassan, "Dual axis solar tracker for solar panel with wireless switching," in *Proc. Int. Conf. Microelectron., Comput. Commun. Syst. (MCCS)*, 2019, pp. 49–62, doi: 10.1007/978-981-10-8234-4_6.

[16] Y. Away, Y. Yanti, M. S. Rizal, and A. Novandri, "Interactive control using Bluetooth for dual axis sun tracker with three light sensors," in *Proc. Int. Conf. Educ., Sci. Technol.*, 2019, pp. 1–9, doi: 10.1088/1742-6596/1232/1/012038.

[17] H. Fathabadi, "Novel online sensorless dual-axis sun tracker," *IEEE/ASME Trans. Mechatronics*, vol. 22, no. 1, pp. 321–328, Feb. 2017, doi: 10.1109/TMECH.2016.2611564.

[18] H. Fathabadi, "Comparative study between two novel sensorless and sensor based dual-axis solar trackers," *Sol. Energy*, vol. 138, pp. 67–76, Nov. 2016, doi: 10.1016/j.solener.2016.09.009.

[19] M. Mishra and M. Srivastava, "A view of artificial neural network," in *Proc. Int. Conf. Adv. Eng. Technol. Res.*, Aug. 2014, pp. 1–3, doi: 10.1109/ICAETR.2014.7012785.

[20] R. A. Purba, S. Samsir, M. Siddik, S. Sondang, and M. F. Nasir, "The optimalization of backpropagation neural networks to simplify decision making," *IOP Conf. Ser., Mater. Sci. Eng.*, vol. 830, no. 2, 2020, Art. no. 022091, doi: 10.1088/1757-899X/830/2/022091.

[21] X. Sui, Q. Wu, J. Liu, Q. Chen, and G. Gu, "A review of optical neural networks," *IEEE Access*, vol. 8, pp. 70773–70783, 2020, doi: 10.1109/ACCESS.2020.2987333.

[22] E. Vamsidhar, K. V. S. R. P. Varma, P. S. Rao, and R. Satapati, "Prediction of rainfall using backpropagation neural network model," *Int. J. Comput. Sci. Eng.*, vol. 2, no. 4, pp. 1119–1121, 2010.

[23] N. K. Singh, S. S. Badge, and G. F. Salimath, "Solar tracking for optimizing conversion efficiency using ANN," in *Proc. 6th Int. Conf. FICTA*, 2018, pp. 551–559, doi: 10.1007/978-981-10-7566-7.

[24] S. Li, H. Huang, and W. Lu, "A neural networks based method for multivariate time-series forecasting," *IEEE Access*, vol. 9, pp. 63915–63924, 2021, doi: 10.1109/ACCESS.2021.3075063.

[25] S. Marinai, M. Gori, and G. Soda, "Artificial neural networks for document analysis and recognition," *IEEE Trans. Pattern Anal. Mach. Intell.*, vol. 27, no. 1, pp. 23–35, Jan. 2005, doi: 10.1109/TPAMI.2005.4.

[26] V. Kumar, P. Gaur, and A. P. Mittal, "ANN based self tuned PID like adaptive controller design for high performance PMSM position control," *Exp. Syst. Appl.*, vol. 41, no. 17, pp. 7995–8002, Dec. 2014, doi: 10.1016/j.eswa.2014.06.040.

[27] Y. Away, H. Walidainy, M. S. Rizal, and A. Novandri, "Artificial neural network technique to predict the sun position in cloudy state with tetrahedron based sensor," in *Proc. Int. Conf. Comput. Syst., Inf. Technol., Electr. Eng. (COSITE)*, Oct. 2021, pp. 134–137, doi: 10.1109/COSITE52651.2021.9649550.

[28] Z. Chen, H. Zha, K. Peng, J. Yang, and J. Yan, "A design method of optimal PID-based repetitive control systems," *IEEE Access*, vol. 8, pp. 139625–139633, 2020, doi: 10.1109/ACCESS.2020.3012506.

[29] J. Li and W. Li, "On-line PID parameters optimization control for wind power generation system based on genetic algorithm," *IEEE Access*, vol. 8, pp. 137094–137100, 2020, doi: 10.1109/ACCESS.2020.3009240.

[30] M. Melinda, A. Novandri, and Y. Away, "PID controllers performance on dual axis tracking with tetrahedron based sensor," *Kinetik, Game Technol., Inf. Syst., Comput. Netw., Comput., Electron., Control*, vol. 7, pp. 371–382, Nov. 2022, doi: 10.22219/kinetik.v7i4.1549.

[31] C. A. Aung, Y. V. Hote, G. Pillai, and S. Jain, "PID controller design for solar tracker via modified ziegler nichols rules," in *Proc. 2nd Int. Conf. Smart Power Internet Energy Syst. (SPIES)*, Sep. 2020, pp. 531–536, doi: 10.1109/SPIES48661.2020.9243009.

[32] M. M. Sabir and T. Ali, "Optimal PID controller design through swarm intelligence algorithms for sun tracking system," *Appl. Math. Comput.*, vol. 274, pp. 690–699, Feb. 2016, doi: 10.1016/j.amc.2015.11.036.

[33] I. Abadi, A. Musyafa', W. Z. Putra, and D. N. Fitriyanah, "Performance analysis of dual axis solar tracker based on fuzzy PID controller on street lighting," in *Proc. Int. Conf. Comput. Eng., Netw., Intell. Multimedia (CENIM)*, Nov. 2020, pp. 257–263, doi: 10.1109/CENIM51130.2020.9297938.

[34] S. Gupta and J. K. Mohanta, "Design of PID controller using artificial neural network for step-up power converter in photovoltaic systems," in *Proc. Int. Conf. Power, Instrum., Energy Control (PIECON)*, Feb. 2023, pp. 1–6, doi: 10.1109/PIECON56912.2023.10085911.

[35] N. Hassan and A. Saleem, "Neural network-based adaptive controller for trajectory tracking of wheeled mobile robots," *IEEE Access*, vol. 10, pp. 13582–13597, 2022, doi: 10.1109/ACCESS.2022.3146970.

[36] K. H. Al-Waeli, R. Ramli, S. M. Haris, Z. B. Zulkoffli, and M. S. Amiri, "Offline ANN-PID controller tuning on a multi-joints lower limb exoskeleton for gait rehabilitation," *IEEE Access*, vol. 9, pp. 107360–107374, 2021, doi: 10.1109/ACCESS.2021.3101576.

[37] O. Rodríguez-Abreo, J. Rodríguez-Reséndiz, C. Fuentes-Silva, R. Hernández-Alvarado, and M. D. C. P. T. Falcón, "Self-tuning neural network PID with dynamic response control," *IEEE Access*, vol. 9, pp. 65206–65215, 2021, doi: 10.1109/ACCESS.2021.3075452.

[38] K. Kumari, G. Shankar, S. Kumari, and S. Gupta, "Load frequency control using ANN-PID controller," in *Proc. IEEE 1st Int. Conf. Power Electron., Intell. Control Energy Syst. (ICPEICES)*, Jul. 2016, pp. 1–6, doi: 10.1109/ICPEICES.2016.7853516.

[39] R. Hernández-Alvarado, L. G. García-Valdovinos, T. Salgado-Jiménez, A. Gómez-Espinosa, and F. Fonseca-Navarro, "Neural network-based self-tuning PID control for underwater vehicles," *Sensors*, vol. 16, no. 9, pp. 1–18, 2016, doi: 10.3390/s16091429.

[40] C. Uchegbu, I. Eneh, M. Ekwuribe, and C. Ugwu, "Remoldelling of PID controller based on an artificial intelligency (neural network)," *Amer. J. Sci., Eng. Technol.*, vol. 1, no. 2, pp. 20–26, 2016, doi: 10.11648/j.ajset.20160102.12.

[41] S.-G. Cui, H.-L. Pan, and J.-G. Li, "Application of self-tuning of PID control based on BP neural networks in the mobile robot target tracking," in *Proc. 3rd Int. Conf. Instrum., Meas., Comput., Commun. Control*, Sep. 2013, pp. 1574–1577, doi: 10.1109/IMCCC.2013.350.

[42] M. Aamir, "On replacing PID controller with ANN controller for DC motor position control," *Int. J. Res. Stud. Comput.*, vol. 2, no. 1, pp. 21–29, Apr. 2013, doi: 10.5861/ijrsc.2013.236.

[43] W. Lu, J. H. Yang, and X. D. Liu, "The PID controller based on the artificial neural network and the differential evolution algorithm," *J. Comput.*, vol. 7, no. 10, pp. 2368–2375, Oct. 2012, doi: 10.4304/jcp.7.10.2368-2375.

[44] M. Madheswaran and M. Muruganandam, "Simulation and implementation of PID-ANN controller for chopper fed embedded PMDC motor," *ICTACT J. Soft Comput.*, vol. 2, no. 3, pp. 319–324, Apr. 2012, doi: 10.21917/ijsc.2012.0049.

[45] B. V. Murthy, Y. V. P. Kumar, and U. V. R. Kumari, "Application of neural networks in process control: Automatic/online tuning of PID controller gains for ±10% disturbance rejection," in *Proc. IEEE Int. Conf. Adv. Commun. Control Comput. Technol. (ICACCCT)*, Aug. 2012, pp. 348–352.

[46] O. A. Dahunsi, J. O. Pedro, and O. T. Nyandoro, "System identification and neural network based PID control of servo—Hydraulic vehicle suspension system," *SAIEE Afr. Res. J.*, vol. 101, no. 3, pp. 93–105, Sep. 2010, doi: 10.23919/saiee.2010.8531554.

[47] P. Shah and S. Agashe, "Review of fractional PID controller," *Mechatronics*, vol. 38, pp. 29–41, Sep. 2016, doi: 10.1016/j.mechatronics.2016.06.005.

[48] H. O. Bansal, R. Sharma, and P. R. Shreeraman, "PID controller tuning techniques: A review," *J. Control Eng. Technol.*, vol. 2, pp. 168–176, May 2012.

[49] M. Kushwah and A. Patra, "PID controller tuning using Ziegler-Nichols method for speed control of DC motor," *Int. J. Sci. Eng. Technol. Res.*, vol. 3, no. 13, pp. 2924–2929, 2014.

[50] H. Wu, W. Su, and Z. Liu, "PID controllers: Design and tuning methods," in *Proc. 9th IEEE Conf. Ind. Electron. Appl.*, Jun. 2014, pp. 808–813, doi: 10.1109/ICIEA.2014.6931273.

[51] W. Wang and Y. Lu, "Analysis of the mean absolute error (MAE) and the root mean square error (RMSE) in assessing rounding model," *IOP Conf. Ser., Mater. Sci. Eng.*, vol. 324, no. 1, 2018, Art. no. 012049, doi: 10.1088/1757-899X/324/1/012049.

[52] T. Chai and R. R. Draxler, "Root mean square error (RMSE) or mean absolute error (MAE)?—Arguments against avoiding RMSE in the literature," *Geoscientific Model Develop.*, vol. 7, no. 3, pp. 1247–1250, Jun. 2014, doi: 10.5194/gmd-7-1247-2014.

[53] S. Sridhar, M. Fazelpour, A. S. Gill, and J. D. Summers, "Accuracy and precision analysis of the graph complexity connectivity method," *Proc. CIRP*, vol. 44, pp. 163–168, Jan. 2016, doi: 10.1016/j.procir.2016.02.029.

[54] P.-T. Wilrich, "Robust estimates of the theoretical standard deviation to be used in interlaboratory precision experiments," *Accreditation Quality Assurance*, vol. 12, no. 5, pp. 231–240, May 2007, doi: 10.1007/s00769-006-0240-7.

[55] M. C. DeSantis, S. H. DeCenzo, J.-L. Li, and Y. M. Wang, "Precision analysis for standard deviation measurements of immobile single fluorescent molecule images," *Opt. Exp.*, vol. 18, no. 7, p. 6563, 2010, doi: 10.1364/oe.18.006563.

[56] P. Trebuna, J. Halcinová, M. Fil'o, and J. Markovic, "The importance of normalization and standardization in the process of clustering," in *Proc. IEEE 12th Int. Symp. Appl. Mach. Intell. Informat. (SAMI)*, Jan. 2014, pp. 381–385, doi: 10.1109/SAMI.2014.6822444.

[57] M. Ahsanullah, B. M. G. Kibria, and M. Shakil, *Normal and Student's T Distributions and Their Applications* (Atlantis Studies in Probability and Statistics), vol. 4. Dordrecht, The Netherlands: Atlantis Press, 2014, pp. 7–50.

[58] I. D. Madaki, T. A. Folorunso, J. A. Bala, A. Peace, and E. M. Dogo, "Performance evaluation of sun tracking control systems using IMC and PID controllers," in *Proc. 4th Int. Eng. Conf. (IEC)*, 2022, pp. 89–94.

[59] Z. A. Yusuf, A. T. Salawudeen, and H. Bege. (2019). *Tracking and Control of DC Motor for PV Systems Positioning Using Artificial Bee Colony Algorithm*. [Online]. Available: https://www.academia.edu/download/65461382/solar2018.pdf

[60] B. O. Oladayo and A. O. Titus, "Development of solar tracking system using IMC-PID controller," *Amer. J. Eng. Res.*, vol. 5, no. 5, pp. 135–142, 2016.

[61] F. Rahmah, F. Hidayanti, E. K. Wati, K. R. Lestari, and S. W. Sudrajat, "Solar panel motor tracker model comparison between PID and fuzzy PD," *Int. J. Renew. Energy Res.*, vol. 12, no. 3, pp. 1427–1434, 2022, doi: 10.20508/ijrer.v12i3.13117.g8525.

**YUWALDI AWAY** (Member, IEEE) was born in South Aceh, Indonesia, in 1964. He received the degree in electrical-computer engineering from the Sepuluh Nopember Institute of Technology (ITS), Indonesia, in 1988, the M.Sc. degree from the Bandung Institute of Technology (ITB), Indonesia, in 1993, and the Ph.D. degree in industrial computer from the National University of Malaysia, in 2000. Since 1990, he has been a Lecturer with the Department of Electrical Engineering, Faculty of Engineering, Syiah Kuala University, Indonesia. He was a Research Assistant and a Lecturer with the National University of Malaysia, from 2001 to 2004. Since 2007, he has been a Professor and the Head of Research Group for Automation and Robotics Studies, Syiah Kuala University. His research interests include the combination of theory and practical, including microprocessor-based systems, simulation, automation, and optimization.

**ANDRI NOVANDRI** (Student Member, IEEE) was born in Aek Kanopan, North Sumatera, Indonesia, in 1994. He received the Bachelor of Engineering degree in electrical and computer engineering and the Master of Engineering degree from Syiah Kuala University, Indonesia, in 2017 and 2023, respectively. Since 2018, he has been active as a Research Assistant with Syiah Kuala University. After graduating with his master's degree, in 2023, he began actively teaching as a Lecturer with the Department of Information Technology, Faculty of Science and Technology, Ar-Raniry State Islamic University, Indonesia. His research interests include embedded systems, robotics, automation and control systems, sensors, and machine learning.

**ISYATUR RAZIAH** (Student Member, IEEE) was born in 1995. She received the bachelor's and master's degrees in electrical and computer engineering from Syiah Kuala University, Banda Aceh, Indonesia, in 2018 and 2020, respectively, and the Ph.D. degree in engineering, in 2023. Since 2022, she has been a Lecturer with the Department of Information Technology, Faculty of Engineering, Teuku Umar University, Indonesia. Her research interests include wireless communication systems and device-to-device (D2D) communication.

**MELINDA MELINDA** (Member, IEEE) was born in Bireuen, Aceh, in June 1979. She received the B.Eng. degree from the Department of Electrical Engineering, Faculty of Engineering, Syiah Kuala University, Banda Aceh, in 2002, the master's degree in radio frequency communication systems from the Electrical Department, University of Southampton, U.K., in 2009, and the Ph.D. degree from the Department of Electrical Engineering, Engineering Faculty, Universitas Indonesia, in February 2018. She has been with the Department of Electrical Engineering, Faculty of Engineering, Syiah Kuala University, since 2002. Her research interests include signal and fluctuation processing.